Cement and Concrete Research 88 (2016) 96–107

Contents lists available at ScienceDirect

Cement and Concrete Research

journal homepage: www.elsevier.com/locate/cemconres

Chloride-induced corrosion of reinforcement in low-calcium fly ash-based geopolymer concrete

M. Babaee *, A. Castel

Centre for Infrastructure Engineering and Safety, School of Civil and Environment Engineering, University of New South Wales Sydney, NSW, 2052, Australia

ARTICLE INFO

Article history:
Received 22 May 2015
Received in revised form 16 May 2016
Accepted 18 May 2016
Available online 24 June 2016

Keywords:
Geopolymer concrete
Low-calcium fly ash
Durability
Corrosion

ABSTRACT

Geopolymer concrete (GPC) has significant potential as a more sustainable alternative for ordinary Portland cement concrete (PCC). However; as a rather new engineering material, there are some concerns over the durability aspects of geopolymer-based binders. In this study, the performance of chloride-contaminated reinforced GPC specimens manufactured using a blended low-calcium fly ash and slag cement is investigated by long-term monitoring of corrosion parameters such as open circuit corrosion potential, polarization resistance and Tafel slopes. The electrochemical results are validated by contrasting the electrochemical mass losses with the mass losses obtained from the gravimetric measurements. The investigated low-calcium fly ash-based GPC exhibit a comparable electrochemical performance to a similar strength PCC during the propagation phase of corrosion. Additionally, some of the conventional classifications which are commonly used to assess the severity of corrosion in Portland cement-based corroding systems might need some recalibration to be used for low-calcium fly ash-based corroding systems.

1. Introduction

Ordinary Portland cement concrete (PCC) is the most commonly used material in the construction industry [1] and global demand for it is projected to increase steeply until 2050 reaching 5.5 Gt/year [2]. Concrete is indeed an attractive construction material regarding mechanical performance, durability, shape adaptability and availability of raw precursors. Nonetheless, production of PCC is associated with some significant environmental impacts such as massive consumption of natural resources and responsibility for as much as 6–7% of all the greenhouse gasses emitted worldwide [3–5].

PCC can be prone to degradation and premature failure and using Portland cement-based concretes can lead to serious problems with millions of dollars spent for maintenance, repair or replacement of damaged structures [6–8]. In this regard, developing alternative binders can be considered as an efficient way of overcoming the hurdles associated with the production and application of Portland cement binders. Among all the available alternative binders, geopolymer binders have a great development potential and are widely considered as a promising alternative for Portland cement binders [9]. Geopolymer binders are produced by the chemical reaction of alumina-silicate oxides with alkali polysilicates to produce polymeric Si—O—Al bonds [10]. Due to the low cost and wide availability, industrial waste materials such as fly ash are commonly used as the source of aluminosilicate for the manufacture of geopolymer concrete (GPC).

While emitting up to nine times less carbon dioxide [11], GPCs exhibit many of the engineering characteristics of traditional concretes, despite their vastly different chemical composition and reaction mechanisms [12–14]. Moreover, geopolymer binders can display other benefits as well, such as higher stability when exposed to elevated temperature [15], higher resistance against chemical attacks [16–18] and better resistance to freeze-thaw cycles [19,20]. However, being a comparatively young engineering material, the quantity of available durability data (crucial for predicting the service life of reinforced GPC structures) such as chloride ingress properties or corrosion rate of embedded reinforcing steels is limited, and the long-term performance of GPC structures is yet to be determined [9,21].

Low-calcium fly ash-based (Class F) GPC has been reported by some researchers to have lower chloride diffusion coefficients, chloride content and porosity compared to high-calcium (Class C) fly ash-based GPC and PCC [22], while others have found that the exact raw materials and mixture design can result in varying performance [23]. Lloyd et al. [24] concluded that the presence of calcium is essential to lower the permeability of pore system and prevent alkalis from leaching and consequent pH drop which can lead to depassivation of embedded reinforcement. Previous studies reveal that due to the high alkalinity of the pore system, fly ash based GPC can passivate the reinforcement steel as efficiently as PCC [24–28]. Type and concentration of the alkaline solution have also been found to play a crucial role in the stability of passive film [1,24,28]. While performance of fly ash-based GPC is

* Corresponding author.
E-mail addresses: mahdi.babaee@unsw.edu.au (M. Babaee), a.castel@unsw.edu.au (A. Castel).

http://dx.doi.org/10.1016/j.cemconres.2016.05.012
0008-8846/

observed to be similar to PCC in passive state (i.e. in the absence of chloride ions) [25,28], an (at least) equivalent performance of low-calcium fly ash-based GPC compared with PCC in severe marine environments during the propagation phase of corrosion is emphasized [28–30].

Considering the limited literature available related to the chloride-induced corrosion of reinforcements in geopolymer concretes, this work aims to:

- Assess the performance of low-calcium fly ash-based GPC during the propagation phase of corrosion process through long-term monitoring of corrosion parameters such as open circuit corrosion potential, polarization resistance and Tafel coefficients. The results are compared with the reported values for PCC. Direct mass loss measurement is carried out as a way to validate results of the corrosion tests.
- find out if the existing electrochemical test methods calibrated and validated for reinforced Portland cement concrete are suitable for geopolymer concrete.

2. Experimental program

2.1. Geopolymer concrete mix design and precursors

An experimental investigation is conducted to assess the corrosion of reinforced GPC fabricated from a blend of Class F fly ash and ground granulated blast-furnace slag (GGBFS) stockpiles. In accordance with a previous study [31], three different sources of aluminosilicate precursors have been used: 1 - fly ash (FA) from Eraring Power Station (New South Wales, Australia), 2 - an ultra-fine FA branded as Kaolite high-performance ash (HPA), sourced from Callide Power Station (Queensland, Australia), and 3 - ground granulated blast-furnace slag (GGBFS) supplied by Blue Circle Southern Cement Australia. Both fly ashes are low-calcium class F fly ash (ASTM C 618 Class F). Chemical compositions of the aluminosilicate sources determined by X-ray fluorescence (XRF) analysis are listed in Table 1.

A mixture of the sodium hydroxide (NaOH) solution and sodium silicate (Na_2SiO_3) solution was used [31,32]. The sodium hydroxide solution used was prepared by dissolving the technical grade NaOH pellets in water. The sodium hydroxide white pellets with a purity of at least 98% were supplied by Ajax Finechem under the commercial name of UNIVAR A-302. These pellets have a specific gravity of 2.1 g/cm^3 and a pH of approximately 14. The concentration of sodium hydroxide solution used is 12 M (12 M) which consisted of 480 g of NaOH pellets per liter of solution or 361 g of NaOH pellets per kg of solution. Grade D sodium silicate, which was supplied by PQ Australia under the commercial name of Vistrol D–A53, has a chemical composition of Na_2O = 14.7%, SiO_2 = 29.4% and H_2O = 55.9% (by mass). The Na_2SiO_3 solution used is a thick adhesive liquid with a viscosity of 400 cps at 20 °C, has a specific gravity of 1.53 g/cm^3 and a pH of 12.9 (values provided by the supplier, PQ Australia). Also, the ratio of sodium silicate to sodium hydroxide solution used was 2.5:1 (by mass) to maximize the compressive strength, while having an acceptable workability and pH level [33–35]. The modulus (the molar ratio of SiO_2/Na_2O) of the solution is 1.17.

Mix proportioning of the raw material ingredients, as shown in Table 2, was carried out by mass. About 85% of the blend is composed of low-calcium class F fly ash. Sydney sand was used as fine aggregate, and the coarse aggregate was 10 mm nominal size crushed basalt. The aggregate's mass shown in Table 2 is in the saturated surface dry (SSD) condition.

2.2. Fabrication of specimens, curing and exposure condition

To prohibit any external corrosion, a specific method of fabrication has been adopted (Fig. 1), similar to the approaches employed in some previous studies to assess the steel corrosion in PCC [36,37]. The reinforcing bars used were normal ductility grade 12 mm deformed bars with 500 MPa yield strength. All embedded bars were 50 mm long and were machined at both ends. Rebars were gently wire-brushed to eliminate any pre-formed rusts which could affect the gravimetric mass loss calculations. All steel bars were then weighed and tagged for gravimetric mass loss measurements at the end of the testing period (after doing the destructive Tafel test on each sample). One acrylic tube was attached at each end. The internal diameter of the acrylic tubes was almost equal to the external diameter of the machined part of the steel bars, so the steel bar could easily fit in the tube, although a thin layer of silicone sealant was used as an adhesive and also to avoid any corrosion on the machined parts of the steel bars. Acrylic tubes were then filled with Silicone sealant to block the access for chloride ions to the steel bar (Fig. 1). A copper wire was welded on each steel bar to perform as a working electrode during the electrochemical measurements. Both top and bottom sides of samples were coated with an *anti*-chloride resin (supplied by the Australian supplier "Parchem" under the commercial name of Emer-Stop S100 N), to enforce peripheral penetration of chloride ions.

After casting, moulds were sealed with either a proper lid or a plastic sheet to prevent excessive loss of moisture and were stored in a chamber at 40 °C for 24 h. The specimens were then demoulded, sealed again and placed in a hot water bath at 80 °C for another 24 h. After that, samples were stored in a room with a fixed temperature of 23 ± 2 °C and relative humidity (RH) of 50% until the testing dates. The average compressive strength (average of 3 samples) at 28th day was 54.5 MPa with a standard deviation of 1.10 MPa. Also, the average elastic modulus (average of 3 samples) at 28th day was 23.8 GPa with a standard deviation of 0.61 GPa.

Table 1
Chemical compositions of FA, kaolite HPA and GGBFS by X-ray fluorescence (XRF) analysis.

Oxide	FA [wt.%]	Kaolite HPA [wt.%]	GGBFS [wt.%]
Silicon dioxide (SiO_2)	66.56	45.14	31.52
Aluminium oxide (Al_2O_3)	22.47	33.32	12.22
Iron oxide (Fe_2O_3)	3.54	11.99	1.14
Calcium oxide (CaO)	1.64	4.13	44.53
Potassium oxide (K_2O)	1.75	0.13	0.33
Sodium oxide (Na_2O)	0.58	0.07	0.21
Magnesium oxide (MgO)	0.65	1.37	4.62
Manganese oxide (MnO)	0.06	0.23	0.36
Phosphorus oxide (P_2O_5)	0.11	0.56	0.02
Titanium oxide (TiO_2)	0.88	2.19	1.03
Sulphur trioxide (SO_3)	0.10	0.48	3.24
Loss of ignition (LOI)	1.66	0.41	0.79
Specific gravity	2.1	2.4	2.8

Table 2
GPC mix proportions.

Material	kg/m^3
Coarse aggregate	1138
Fine aggregate	730
FA	200
Kaolite HPA	55
GGBFS	45
12 M sodium hydroxide solution (NaOH)	45.7
Sodium silicate solution (Na_2SiO_3)	114.3
Free water	31
Coarse aggregate/fine aggregate	1.60
Total binder (FA, HPA, GGBFS)	300
Water/binder[1]	0.35
Modulus (SiO_2/Na_2O)	1.17
Na_2O/binder (wt.%)	9.86

[1] Calculated considering the total water and the total solids (precursors + anhydrous activator).

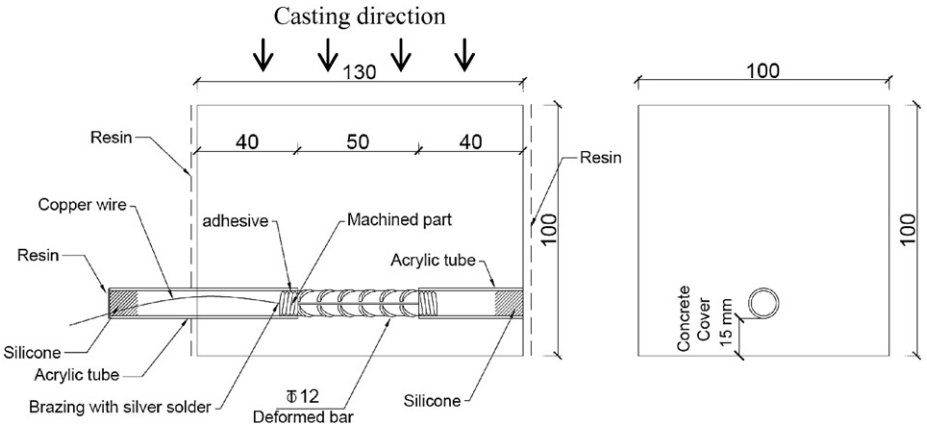

Fig. 1. GPC specimen configuration.

The initiation period of the chloride-induced corrosion process (i.e. chloride penetration through the concrete cover) was accelerated as the study focuses on the steel corrosion during the propagation phase of corrosion. 28 days after casting, 11 specimens were partially dried in an oven at 50 °C to enhance capillary suction before the first immersion in a 35 g/L sodium chloride solution, which is similar to the concentration of the seawater. This method has been already used for Portland cement concretes successfully to accelerate the initiation phase of corrosion [37]. After that, specimens were subjected to alternating wetting/drying cycles during the whole testing period (almost 11 months), immersed in the sodium chloride solution for one week, followed by at least two weeks of air exposure under a fixed temperature of 23 ± 2 °C and RH of 50%. Alongside with the samples whose initiation phase of corrosion was accelerated, six samples were submerged in tap water for almost seven weeks to be saturated and used for passive condition corrosion assessment.

2.3. Electrochemical experiments

All tests have been carried out in a room with a fixed temperature of 23 °C. Corrosion parameters such as the open circuit corrosion potential (E_{corr}), polarization resistance (R_p) and Tafel constants have been measured and the obtained results were validated by comparing the gravimetric and electrochemical mass losses. Also, Gravimetric measurements were beneficial to calibrate R_p measurements regarding finding an appropriate potential sweep rate range [38,39]. pH of the samples was measured as the passivity of steel bar depends on the pH of the concrete. Chloride content measurements were carried out as well using the ion chromatography (IC) technique.

To carry out all the electrochemical tests, a three-electrode system was used comprising of a Saturated Calomel Electrode (SCE) as the reference electrode (RE), a Titanium mesh as the counter electrode (CE) and the reinforcing bar as the working electrode (WE). During the corrosion tests, samples have been placed partially in water, they were not completely submerged to avoid concentration polarization due to the lack of oxygen. RE and CE were also put in the water next to the sample. E_{corr} was determined by open circuit measurement of the potential difference between the WE and RE while the stability of the half-cell potential was controlled beforehand (E_{corr} was monitored but not recorded until the deviation was lower than 1 mV during a 60s period) [40].

The most widespread technique to evaluate the corrosion current (I_{corr}) is the Linear Polarization Resistance (LPR) method which allows calculation of the corrosion rate via the Stern-Geary equation [41,42]:

$$I_{corr} = \frac{\beta_a \beta_c}{2.3\, R_p\, (\beta_a + \beta_c)} = \frac{B}{R_p} \tag{1}$$

where β_a and β_c are anodic and cathodic Tafel slopes ($\frac{d\eta}{d\ \log i}$), respectively. Measuring the corrosion potential (E_{corr}) beforehand, R_p can be obtained from the slope of the polarization curve in the vicinity of E_{corr} [42]:

$$R_p = \left(\frac{\Delta E}{\Delta I}\right)_{\Delta E \to 0} \tag{2}$$

In a potentiodynamic test, ΔE is the potential step applied within a limited range of overpotentials ($\eta = E\text{-}E_{corr} = -20$ to $+20$ mV in the current study) to polarize the corrosion system and ΔI is the system response to the potential excitation.

Values of B = 26 and 52 mV are suggested for the active and passive state, respectively and widely used in the corrosion rate estimation of reinforced PCC [42]. However, in the present study, they are obtained from the slope of the anodic and cathodic branch of Tafel plots at large overpotentials ($E\text{-}E_{corr} = -200$ to $+200$ mV). A Tafel plot, which is a plot of log I vs. overpotential ($E\text{-}E_{corr}$), can be utilized to obtain both Tafel slopes and I_{corr} simultaneously by extrapolating the anodic and cathodic linear segments to an intercept of log Icorr through a curve-fitting analysis [43,44]. However, the Tafel test is considered as a destructive test, since the strong level of polarization can trigger some irreversible changes in the WE [45]. Due to this drawback, Tafel tests have been conducted only five and three times for active and passive samples respectively within the whole period of the experimental program (about 48 weeks). E_{corr} and R_p have been monitored on a regular basis at the end of wetting cycles for active samples and after seven weeks of immersion in water for passive samples.

A VMP3 Multi-channel potentiostat was employed to perform all the electrochemical tests. It was capable of compensating the ohmic (IR) drop due to the electrolyte resistance by either Current Interruption (CI) method or ZIR method. ZIR technique is very similar to the Potentiostatic Electrochemical Impedance Spectroscopy (PEIS) technique, except that it is performed at a single frequency. Only 85% of the measured ohmic drop was compensated to avoid oscillation of the instrument [39,46]. IR compensation was always implemented before other electrochemical tests to take into account the effect of uncompensated electrolyte resistance (R_e) on the shape of polarization curves (or Tafel plots) and hence revising R_p, Tafel constants and I_{corr}.

The effect of sweep rate on the polarization behavior and R_p of reinforced PCC systems during potentiodynamic polarization tests has been discussed in detail in [38] and then the same concept was adapted for steel/concrete corrosion systems by González et al. [45] and Martínez and Andrade [39]. González et al. [38] investigated the response of a modified Randles circuit (Fig. 2) to an applied potential sweep, and they found out that the range of sweep rates in which $R_p + R_e$ achieves a constant value, is appropriate to do a potentiodynamic polarization

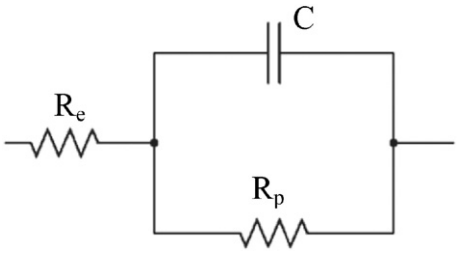

Fig. 2. The modified Randles circuit used by González et al. [38]; R_e is the electrolyte resistance, R_p is the polarization resistance and C is the capacitance of the double layer.

test. Faster sweep rates overestimate the corrosion current (and hence underestimate R_p) as the current bypasses R_p through the capacitor, and the transient component of the intensity is still considerable and cannot be ignored. In this case, the apparent resistance (R_{app}) is equal to the electrolyte resistance (R_e) which is less than the actual resistance of $R_p + R_e$. On the other hand, if the sweep rate is too slow, the concentration of ions in the solution layer around the electrode will change which can lead to underestimation of the corrosion current by altering the electrode equilibrium conditions [38,45]. A too long recovering time for the electrode equilibrium potential to return to the initial E_{corr} is a sign of electrode altering which is more common in the case of passive systems and also in diffusion controlled systems.

After determining the apparent resistance $R_{app} = R_p + R_e$ by applying an appropriate sweep rate, R_p can be determined directly from this value if either R_e is known beforehand or $R_e \ll R_p$. To find the suitable sweep rate and to calculate R_e as a way to calibrate the results of IR drop compensation techniques, a similar methodology was adopted in the current study. A set of cyclic voltammetry (CV) tests in a range of ± 10 mV away from E_{corr} and in a wide range of sweep rates from 1 to 500 mV/min was performed to establish the relation between the R_p values and the sweep rates. Then R_e was estimated from the measured resistance at very fast sweep rates (sweep rates which are larger than 100–200 mV/min), while the proper sweep rate was chosen within the range where $R_p + R_e$ attained a constant value.

To validate the results of electrochemical tests, Gravimetric mass loss measurements were conducted [42] on samples which had been already used for Tafel tests based on the ASTM G1–03 protocol [47]. After splitting the samples, reinforcing bars were taken out and lightly brushed with a non-metallic bristle. Then they were immersed for about 20 min in a chemical solution composed of 1000 mL hydrochloric acid (HCL, sp. gr 1.19), 20 g antimony trioxide (Sb_2O_3) and 50 g stannous chloride ($SnCl_2$). During the immersion, the cleaning solution was vigorously agitated, and the bars were removed from it alternatively, and lightly brushed to ease removing the solidly adhered corrosion products. Only reagent grade chemicals were used to prepare the cleaning solution. After treatment, all the bars were brushed again, rinsed and dried and their masses were measured consequently. This process was repeated several times to obtain a plotted function of mass loss vs. number of cycles for each bar; the mass loss corresponds to the point where the graph begins to plateau. Also to measure the mass of the available oxide layer around the bars, applying the same treatment to 3 replicate uncorroded controlling reinforcing bars resulted in a mass loss of 0.083 g in average with a standard deviation (SD) of 0.0078. This mean value was then deducted from the total measured mass loss to get the actual mass loss due to the chloride-induced corrosion.

2.4. Chloride content

To obtain the total chloride content of concrete (% per binder mass), powder samples were extracted using a German Instrument profile grinder (PF-1100). The test protocol of "ASTM C1152: Standard Test Method for Acid-Soluble Chloride in Mortar and Concrete" [48] is followed and adapted for the ion chromatography (IC) method: five grams of the extracted powder was weighed to the nearest 0.01 g and dispersed with 75 mL water in a beaker. 25 mL (1 + 1) diluted reagent grade Nitric acid was gradually added to the solution afterward, and the final solution was stirred using a magnetic stirrer for 20 min. The solution was rapidly brought to a boil on a hot plate and after cooling down was filtered through a Millex-GS syringe membrane filter (0.22 μm pore size) to remove fine particles. The filtered solution was then diluted to an appropriate mark and analyzed by an ICS-3000 ion chromatography system supplied by Dionex (Sunnyvale, CA, USA).

2.5. pH of geopolymer concrete

The pH of concrete is critical for protecting the steel bars against corrosion, and it is about 13 for uncarbonated Portland cement binders. The pH was measured for a GPC sample and compared to the pH of Portland cement concretes to explain the differences observed in the corrosion potential of passive samples. pH profile of an uncarbonated GPC sample was measured using the suspension method proposed by Räsänen & Penttala [49]. For pH profile measurement, concrete powder samples were taken along the cover depth using the German Instrument profile grinder, 28 days after the heat curing. The sample has been in ambient condition during that period. A suspension mixture was made which was comprised of 50% concrete powder and 50% de-ionised water. Then the suspensions were stirred for 5 min on a magnetic stirrer and finally the pH values were measured using a pH meter. To validate the results, the pore solution from a paste sample (with the same mix design as Table 2 but without aggregates and also with the same curing condition as the geopolymer concrete samples in this study) was extracted and its pH was measured [50]. The maximum applied pressure on the extraction apparatus was 500 MPa and the load rate was 1 MPa/s. As it has already been observed for PCCs [49], the pH value measured by pore solution extraction method was less than the pH values measured using the water suspension method. The difference was about 0.67 which was subtracted from each data point along the profile to obtain the calibrated profile. Results are presented in the following sections.

3. Results and discussion

3.1. Chloride content

Chloride content at the level of the reinforcing bar is measured for two samples at different ages: after the first day of immersion in NaCl solution, and after six drying/wetting cycles. A chloride content of 0.45% by mass of binder (The mass of binder comprises the masses of fly ash, slag, and HPA) is measured after only one day of immersion in NaCl solution. It is worth reminding that achieving this high level of chloride content within a very short time is due to the high capillary suction induced by oven-drying. Although there is not a consensus among the researchers regarding the chloride threshold (the chloride concentration required to depassivate reinforcements) values in Portland cement concrete yet, the recorded chloride content after one day is higher than the chloride threshold levels of 0.2% and 0.4% by mass of cement suggested by ACI [51] and RILEM [52] respectively. The chloride content after 132 days (after six drying/wetting cycles) has increased by about 29% compared to the value measured after one day which is possibly due to the combined effects of longer exposure time to chloride ions and the wetting/drying cycles.

3.2. Sweep rate effects

As it is previously discussed in Sections 2-3, potentiodynamic tests should be performed at sweep rates which are slow enough to ensure a steady-state condition and are also fast enough to avoid altering the electrode due to the change in the concentration of ions around the electrode [53]. Although the proper sweep rate ranges for PCC systems are already suggested in the literature [39,45], like any other unknown corroding system, preliminary tests for geopolymer concrete-based corroding system are required to establish an appropriate sweep rate range.

To investigate the effect of variation of sweep rate (SR) on polarization behavior of reinforced GPC samples, a set of Cyclic Voltammetry (CV) tests has been carried out on both passive and active samples. A potential excitation in the form of a triangular cycle of amplitude 20 mV was applied on two passive, and two active samples with different sweep rates and the results are summarized in Fig. 3.

Fig. 3(a) is the result of a set of CV tests on a saturated passive sample which has been submerged in water for six months. By increasing the SR, response amplitudes increase and an increase in the slope of the cycles is also noticeable which results in smaller R_p values. A similar trend was also observed for the active samples. Higher sweep rates also increase ΔI, the distance between the recorded responses at zero overpotential. This behavior has been already captured successfully and explicitly formulated by studying a modified Randles circuit [38].

Variation of R_p in a broad range of sweep rates from 1 to 500 mV/min is depicted in Fig. 3(b). The measured R_p of both passive and active samples at very fast sweep rates (sweep rates larger than 100–200 mV/min) approaches a constant value which compares well against the compensated ohmic (IR) drop measured using either ZIR or CI method (Table 3).

Another noteworthy trend is the difference between the R_p values measured at both ends of the sweep rate spectrum. While the difference can be of two orders of magnitudes for passive samples, active samples experience minor changes with the SR variations. Similar behavior is reported for reinforced Portland cement concretes [39,45]. Fig. 3(b) is also used to determine the range of appropriate sweep rates at which all the potentiodynamic tests on active and passive GPC samples are conducted throughout this study. The appropriate range, i.e. the range in which the measured resistance values achieve a constant value, is from 5 to 10 mV/min for active samples. Although the graphs do not show an apparent plateau in the case of passive samples in Fig. 3(b), sweep rates from 2.5 to 10 mV/min seem to be suitable. These ranges are quite comparable with the ranges already suggested for the reinforced PCC [39].

Considering these results, the sweep rate in all the LPR tests have been set as 5 and 10 mV/min for passive and active samples respectively. The necessity of having low sweep rates while doing a potentiodynamic test on passive PCC samples has been discussed in [38,45].

Table 3
Comparison of Re measured by IR-drop compensation and CV tests at fast SRs.

Sample	R_e (kΩ·cm^2) IR drop compensation	R_e (kΩ·cm^2) CV
Passive sample 1	204	189
Passive sample 2	132	125
Active sample 1	51	51
Active sample 2	139	142

3.3. Corrosion potential and pH of geopolymer concrete

Corrosion potential (E_{corr}) is the most general used corrosion index, due to the convenience of measurement either on site or in the laboratories using widely available, well-developed instruments. However, unlike all the other measured variables, E_{corr} is rather a qualitative parameter, and there is no direct correlation between Ecorr and the corrosion current (I_{corr}), which describes the rate of dissolution of steel [25,30,39,54].

Fig. 4 shows the average value of E_{corr} for six passive samples after seven weeks of immersion in tap water, along with the evolution of E_{corr} of 11 already-depassivated (active) samples after almost 11 months of monitoring. The reference values commonly used to evaluate the severity of corrosion in reinforced PCC [54] are presented on the same graph for comparison purposes. Since the active samples were also used to carry out the destructive Tafel test throughout the monitoring period, the average values are representative of only 2 data points at the end of the testing period. To assess the potentials which were measured versus SCE, the reference values in ASTM C876–09 [54] which are versus a Copper-Copper Sulfate Reference Electrode (CSE) are increased by 60 mV, based on the recommendations of ASTM G3-14 [55].

The average value of the measured open circuit corrosion potentials decreases significantly (hundreds of millivolts) with the chloride contamination; this behavior is similar to what have frequently been reported for PCC corroding systems. However, the absolute value of the average corrosion potential of passive specimens is more negative than the range in which reinforced Portland cement concretes considered passive (i.e. Ecorr > −140 mV vs. SCE). The more negative values observed in passive samples are not necessarily indicative of a higher risk of corrosion; this can be attributed to a combination of factors such as a lower pH level [56] in geopolymeric binders compared to Portland cement binders (Fig. 5) and also a lack of oxygen at the steel-

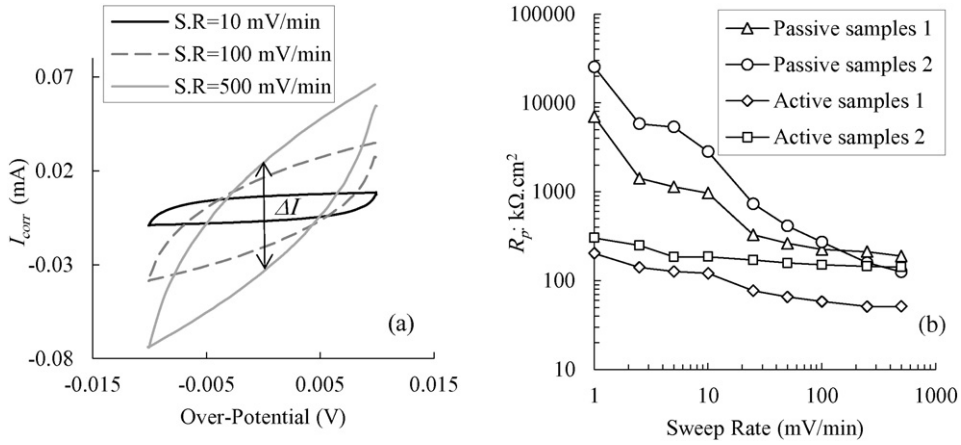

Fig. 3. (a) Response of a passive sample to a triangular wave of potential applied at different sweep rates in a CV test. (b) Variation of Rp with increasing the sweep rates for two passive and two active samples (responses are uncompensated for IR-drop).

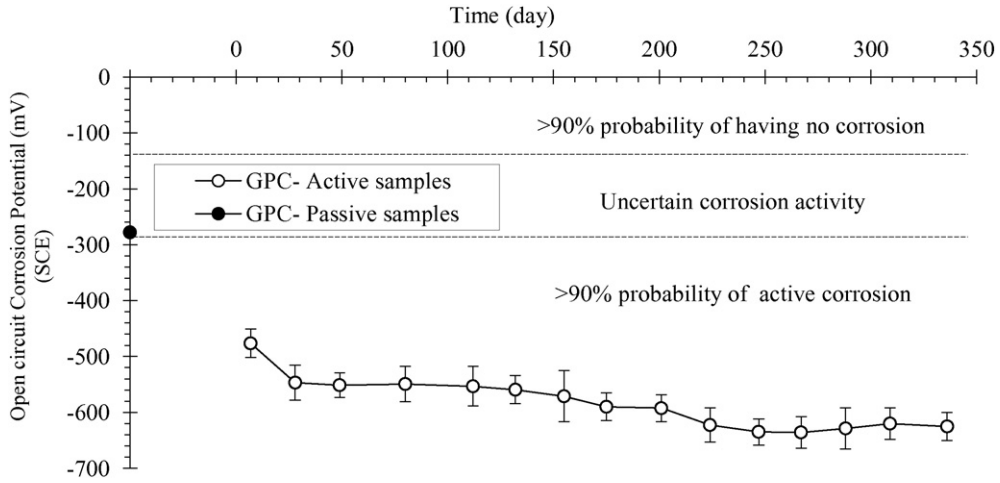

Fig. 4. Evolution of the average open circuit corrosion potential (E_{corr}) along with the standard deviations of each data point and the suggested reference values for PCC [54]. E_{corr} values during the initiation phase are not included, as the initiation phase is accelerated.

concrete interface due to the saturation. Another reason might be the very fine porosity of fly ash binder which decreases the permeability of the binder against oxygen diffusion, and could limit the accessibility of oxygen in cathodic areas which leads to more negative corrosion potential values [1,57–59].

To investigate the pH level of the geopolymer binder in this research, the pH profile of an uncarbonated GPC sample (Fig. 5) is measured using the suspension method [49] and calibrated by direct measurement of the extracted pore solution. Fig. 5 shows that the pH of the geopolymer binder is around 11.5 at the level of the reinforcing bar compared to the widely accepted pH of about 12.5–13 for uncarbonated Portland cement binder systems. As a result, it can be concluded that the lower initial alkalinity of GPC certainly leads to more negative corrosion potential values compared to the reference values which have been calibrated for PCC corroding systems. The corrosion potential of passive GPC samples is currently under further investigation.

The corrosion susceptibility was also investigated by measuring the corrosion current of two passive samples. In addition to the very low measured corrosion currents, the general shape of the polarization curves around the corrosion potential helped to check that the steel bars in passive samples were still passivated (passive samples have very high Rp values which means the slope of the polarization curve around the corrosion potential is very small compared to active samples). Inconsistency between the results of half-cell potential measurements and corrosion current densities has been already reported for GPC [22,30].

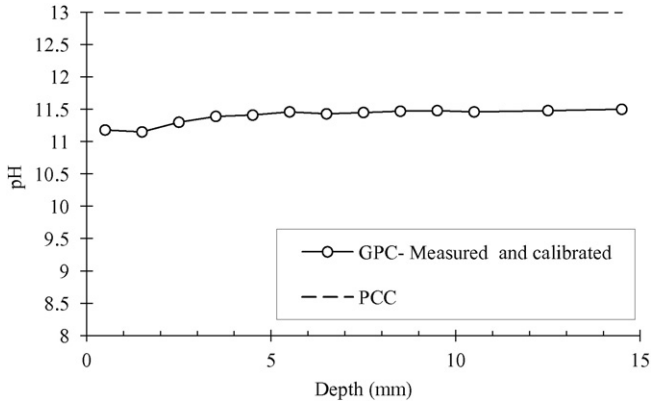

Fig. 5. The calibrated measured pH profile of an uncarbonated GPC vs. the pH value for uncarbonated Portland cement concrete.

For active specimens, due to the low initial corrosion potential and the high chloride content (Sections 3-1), corrosion potentials fall rapidly into the active corrosion zone after only seven days of immersion in NaCl solution. The observed 200 mV drop in the average values after the second wetting cycle is comparable to the potential drop criterion which is used to distinguish between the passive and active steel reinforcements in PCC [60,61]. After 28 days and throughout the testing period, corrosion potential figures fluctuate between −550 and −650 mV vs. SCE, which are slightly more negative than the reported figures for PCC in the literature.

These results draw attention to the intrinsic qualitative nature of the half-cell potential measurements and justify conducting more time-consuming quantitative techniques such as LPR method to assess the state of corrosion reliably. Furthermore, using the conventional reference values of corrosion potential commonly used for PCC increases the possibility of misinterpreting the data while evaluating the passivity of the samples.

3.4. Polarization resistance

Polarizing the working electrode (reinforcing bar) around the measured open circuit corrosion potential (E_{corr}) to obtain the slope of the polarization curve at E_{corr} is a reasonably reliable, yet relatively fast and non-destructive technique to assess the corrosion state. Performing the test within a limited range of potentials, an appropriate sweep rate to achieve a stationary value within a not too long testing time, and the inherent characteristics of steel-concrete systems in which the polarized corrosion system returns to the previous state after only a few hours, are three main factors assuring the system is not undergoing any irreversible alterations. As a result, LPR tests can be repeated on the same sample to monitor corrosion evolving.

Fig. 6 compares the Polarization Resistance (R_p) values of the same specimens of the previous section which are measured at the same time intervals. Reference values of R_p which are widely used to classify the state of corrosion of reinforced Portland cement concretes [62] are also presented in Fig. 6. The reference values are derived by employing Stern-Geary equation (Eq. (1)); a "B″ coefficient equal to 25 is divided by the reference values of corrosion current density suggested by Andrade & Alonso [42]. B = 25 is very close to the recommendation of Andrade & Gonzalez [63] in which they suggested a B value equal to 26 for PCC samples experiencing corrosion. Although "B″ might be of a different value when dealing with Geopolymer concretes (Section 3-5), Rp values are expected to stay within the high corrosion rate range regardless of the further modification of "B″ coefficient. Also, results of a set of tests on PCC samples [37] with a similar fabrication method

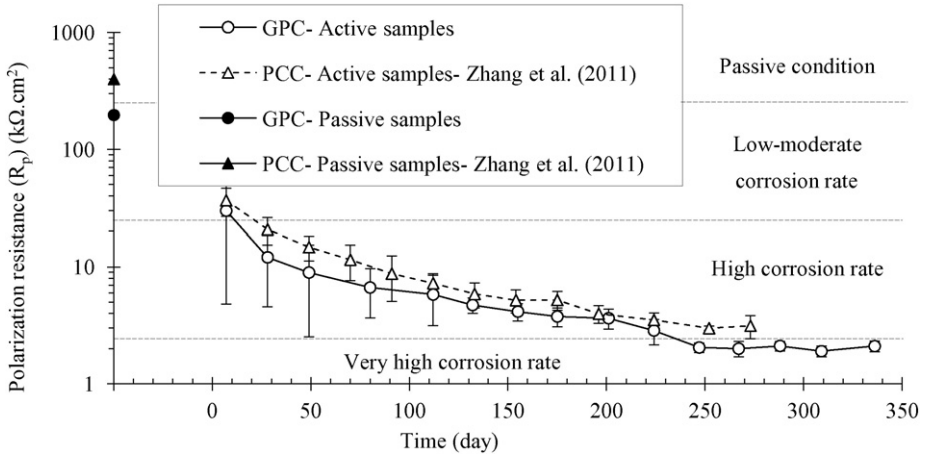

Fig. 6. Evolution of the Polarization Resistance (R_p) along with the standard deviations of each data point and the suggested reference values for PCC. R_p values during the initiation phase are not included, as the initiation phase is accelerated.

and almost the same exposure condition as the current study is presented in Fig. 6. The values reported here from Zhang et al. [37] for PCC samples are average of the results obtained from four specimens.

The average R_p trend is comparable to the corrosion potential trend; the average values reduce significantly (up to 15 times) and fall into the high corrosion rate range after just two cycles of exposure to NaCl solution (samples had been partially dried before the first immersion). The downward trend tends to stabilize toward the end of the testing period, with the average Rp values approaching 2 $k\Omega\cdot cm^2$. Also, the standard deviations and coefficient of variations change from 25.2 and 0.84 respectively after the first wetting cycle to 0.8 and 0.33 at the end. The average polarization resistance trends for GPC and PCC samples exhibit a remarkably good match. As a result, a similar electrochemical performance of Portland cement binders and geopolymer binders in chloride-contaminated environments during the propagation phase of corrosion (after depassivation of reinforcing bars) can be inferred. R_p values measured on passive GPC specimens are slightly lower than the expected values (i.e. $R_p > 250$ $k\Omega\cdot cm^2$ for passive samples). The lower polarization resistance of the passive samples means that to achieve the same anodic or cathodic current level, a smaller overpotential is required. This finding suggests that the PCC classifications might need some recalibration for GPC samples in the passive state.

3.5. Tafel constants

To evaluate the corrosion current density by employing LPR technique and according to (Eq. (1)), besides R_p measurement, two more unknowns should be determined: the anodic Tafel constant ($ß_a$) and the cathodic Tafel constant ($ß_c$). These constants can be calculated from the slopes of the anodic and cathodic branches of the polarization curve which are extrapolated to E_{corr}. This method is known as the "intersection" method [42] or "Tafel extrapolation" method, is also beneficial to determine the corrosion current density (i_{corr}). Although plotting the polarization curve is worthwhile to get some of the most critical parameters defining the kinetic of corrosion, it demands to polarize the sample over a large overpotential range which can introduce some irreversible changes into the system. This justifies the past efforts to figure out some prescribed values for "B″ coefficient to be used in the Stern-Geary equation (Eq. (1)) and hence employing an LPR test in the vicinity of E_{corr} instead of doing the destructive Tafel test. Theoretically, An error factor of less than two is expectable using the Stern-Geary equation to estimate the corrosion current [64].

Corrosion of the reinforcing bars in concrete can be simplistically simulated by its oxidation/reduction reactions in representative solutions. The Tafel slope for oxidation of iron in a basic solution with pH > 13 at 20 °C is about 30–39 mV ($30 < ß_a < 39$). Assuming that reduction of oxygen is the main cathodic reaction at the surface of the reinforcement; the cathodic Tafel slope is highly dependent on the pH of the electrolyte solution and could vary from 48 to 120 mV ($48 < ß_c < 120$). As a result, when the concentration of chloride ions is considerably higher than the chloride threshold, and there is no lack of oxygen (concentration polarization is not rate-determining), B constant for active samples is in the range 8–13.5 ($8 < B < 13.5$). For passive samples, the anodic Tafel slope approaches infinity ($ß_a \to \infty$). Assuming the supply of oxygen is enough, cathodic Tafel slopes are in the same ranges as the active samples ($48 < ß_c < 120$). B constant values in this case range from 21 to 52 ($21 < B < 52$) [65]. The lower conductivity of concrete compared to the solution electrolytes, reduces the rate of transfer of ions into and from the electrolyte (concrete here). A slower charge transfer rate means that a larger potential perturbation is required to achieve the same corrosion rate. Therefore, the Tafel slopes ($d\eta/d\log i$) in concrete are expected to be larger than the values mentioned above for the solution electrolytes.

In a prominent paper, Andrade & Gonzalez (1978) reported results of gravimetric and polarization resistance measurements on mortar samples with embedded reinforcement, manufactured by different types of cement: Portland cement, Slag cement, and Pozzolanic cement. By contrasting the gravimetric losses with the electrochemical mass losses, B values of 26 and 52 for the active and passive state respectively are proposed by Andrade & Gonzalez [63]. Using Eq. (1), $B = 26$ corresponds to $ß_a$ and $ß_c$ values of 120 mV/decade and $B = 52$ could be obtained if $ß_c$ to be 120 mV/decade and the $ß_a$ infinity [44]. Andrade & Gonzalez' suggested figures have been extensively used in practice for reinforced concrete corroding systems, although a wide range of experimentally measured $ß_a$, $ß_c$ and B values can be found in the literature.

Locke and Siman [66] investigated the effect of sodium chloride concentration on corrosion rate and Tafel constants of reinforced concrete samples. Average B constants were ranging from 82 to 278 depending on the sodium chloride content of the concrete, which are much higher than the proposed 52 and 26 for passive and active samples respectively [63]. Locke and Siman argued that the higher observed Tafel slopes are in part due to IR-drop, which was not compensated [66]. The amplifying effect of uncompensated IR-drop on the Tafel slopes of the polarization curve is theoretically discussed in detail in [67]; Although, it is of course insignificant for very low electrolyte resistances [68].

Alonso et al. [69] reported the corrosion current density and Tafel slopes of macrocell beams composed of one chloride containing concrete segment as an anode in the middle and two chloride-free concrete segments as cathodes on both sides of the anode. Macrocell specimens have been in the dry atmosphere for six years, after which they were dampened. The measured anodic Tafel constants ($ß_a$) were approaching infinity while the cathodic Tafel constants were 441 and 289 mV/decade

for the dry and damp beams respectively. The Tafel slopes mentioned above result in B values of 192 and 126 respectively.

Overall, there is an apparent discrepancy in the reported values of Tafel slopes and B constant for OPC based concrete in the literature which comes from a large number of parameters that can affect the Tafel slope figures. These parameters can be listed as: the conductivity of the electrolyte [68] which depends on the moisture content and presence of various ions in the electrolyte, the presence and concentration of chloride ions [66], pH of the electrolyte that can be affected by the carbonation or chemical composition of the electrolyte [70], the polarization mechanism (i.e. activation polarization or concentration polarization) which depends on the availability of the ions involved in redox reactions [65,71], dependency of the Tafel constants on the corrosion potential which varies with time [43,72], the presence of surface films or the mill scale covering the surface of the reinforcement and the surface preparation method [66,73], and pore structure of the concrete which influences the transport properties of different species within the concrete medium. Although chemical composition of the binder (electrolyte) is only one of the many parameters which affect the corrosion kinetic, the polarization curve, and hence the Tafel slopes, given the distinct lack of data on Geopolymer-based corroding systems, measuring the Tafel constants seems to be a necessary step toward developing a database which can be used further in the non-destructive LPR test method.

Fig. 7(a) and (b) show the evolution of the average "B″ coefficient for passive and active state samples after 336 days of immersion in tap water and wetting-drying cycles in NaCl solution respectively. The anodic and cathodic Tafel constants for each data point are also presented in Table 4. To obtain both Tafel constants and the corrosion rate at the same time, the commercial software EC-LAB is used to perform a curve-fitting method. Wellness of the fit is assessed by the Chi-squared (χ^2)test procedure in which χ^2 values are minimized [44].

For passive samples, anodic Tafel slopes approach infinity which is an indication of the passivity of the samples. Also, the cathodic Tafel slopes range between 30 and 45 which results in B coefficients varying from 13 to 20 (as opposed to the conventional B = 52 for PCC samples in the passive state). For active specimens, anodic Tafel constants range between 430 and infinity, while the cathodic Tafel constants range from 106 to 221. These figures result in B coefficients starting at 59 and achieving an average value of 46 after 336 days of immersion in NaCl solution.

The evolution of the polarization curve from the passive state to moderately and then highly active state is depicted in Fig. 8. As it can be seen in Fig. 8 and also Table 4, the anodic Tafel slopes of the active samples show an increasing trend and ultimately approach infinity. The infinite anodic Tafel slopes for corroding samples is also reported in [74]. The very high anodic Tafel slopes in the present study can be attributed to the formation of iron oxide layers around the reinforcing bar. This accumulation of corrosion products slows down the rate of charge transfer and hence the average corrosion rate, as the rate of diffusion of ions involved in the redox reactions into and from the concrete-reinforcement interface reduces. A slower charge transfer rate means higher anodic Tafel slopes, as only a fraction of the applied anodic over-potential is effective to reduce the energy barrier for oxidation of iron.

Table 4
Cathodic and anodic Tafel constants for passive and active samples.

Sample	Time (day)	β_a (mV)	β_c (mV)	B (mV)
Passive samples				
1	42	∞	38	17
2	42	∞	45	20
3	112	∞	40	17
4	112	∞	37	16
5	336	∞	30	13
6	336	∞	32	14
Active samples				
1	7	514	213	65
2	7	536	153	52
3	49	574	221	69
4	49	570	175	58
5	49	430	130	43
6	112	530	153	52
7	112	1107	135	52
8	288	∞	120	52
9	288	∞	133	58
10	336	∞	110	48
11	336	∞	106	45

The presence of an iron oxide layer which is uniformly formed around the reinforcing bars is illustrated in Fig. 11 (Section 3-7). Also, the effect of the formed iron oxide layer on the reduction of the increasing trend of the average corrosion current density with time is discussed in the following section.

3.6. Corrosion current density and mass loss measurement

Fig. 9 depicts the corrosion current densities of GPC samples which are calculated using two different techniques: 1 - the intersection (Tafel extrapolation) method, and 2 - the LPR method (the Stern-Geary equation) using B value of 26 and the average R_p values of all samples at each data point. For comparison purposes, the corrosion current densities of a set of PCC samples from Zhang et al.'s study [37] are calculated from the reported R_p values (Fig. 6), using the Stern-Geary equation and a B coefficient of 26, and the results are also presented in the same figure. All the presented corrosion current density graphs are an

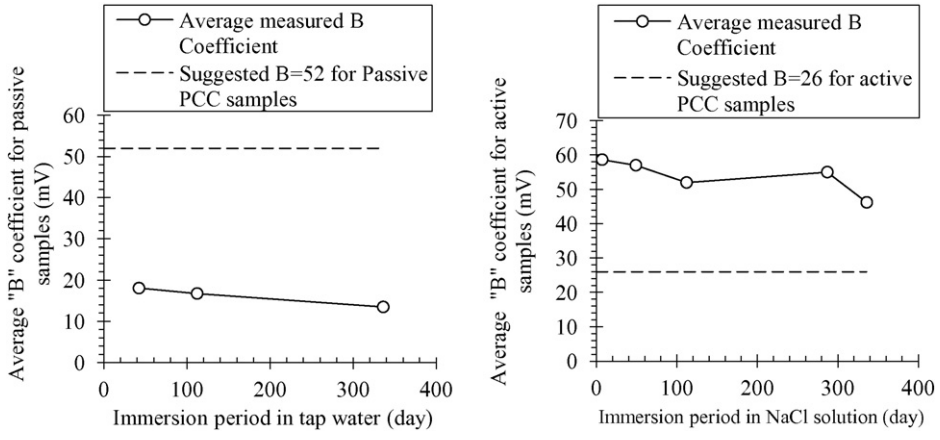

Fig. 7. Variation of the average "B″ coefficients with time for (a) Passive samples and (b) Active samples.

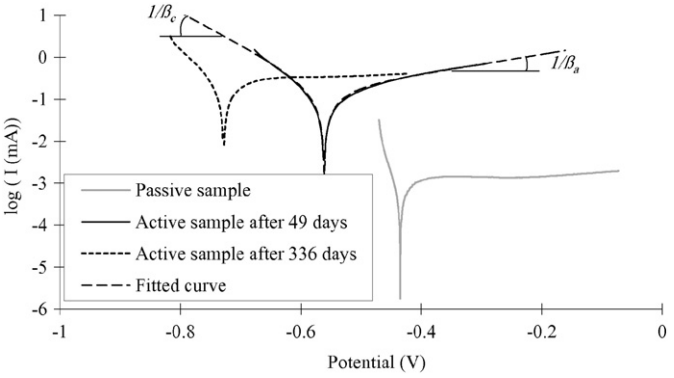

Fig. 8. Polarization curves for passive and active samples.

upper bound for the actual corrosion current densities, as the measurements have been taken place at the end of wetting cycles. As it is shown, the corrosion current density values plateaued with time which is consistent with the high measured anodic Tafel slopes. This behavior can be attributed to the formation of iron oxide layers around the reinforcing bars; more explanations are provided in the previous section.

The corrosion current densities of GPC samples calculated using B = 26 are as low as one-third of the corrosion current densities calculated using the Tafel extrapolation method. This dissimilarity is in part due to the difference in the number of samples used in the calculation of the corrosion current in each method which results in different average R_p values at each data point. The mean R_p value of the two samples tested at each data point for the Tafel slope measurement is not representative of the average Rp of all the samples (refer to Fig. 6 to see the standard deviations of R_p values at each data point). If the same number of samples were used for both methods, the observed difference in the corrosion current density values would be only due to the difference between the measured B values (Table 4) and the prescribed B value of 26 mV. As a result, using the prescribed value of B constant instead of the measured value might introduce a considerable error factor into the system (assuming that the gravimetric and electrochemical mass losses are reasonably close to each other, i.e. electrochemical results are accurate enough). Considering the significant variability of the B constant (Section 3-5), and given all the economic and safety issues associated with an inaccurate estimation of the corrosion rate, having more experimental results to build up a reliable database of B constants to be used in the Stern-Geary equation is strongly recommended.

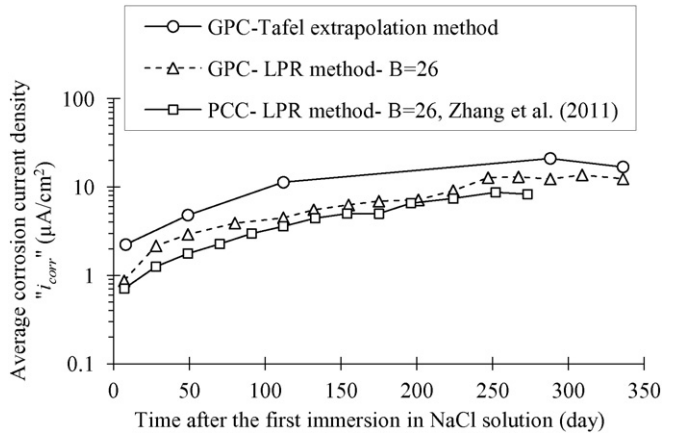

Fig. 9. Average corrosion current density of GPC and PCC samples during the propagation phase of corrosion. (The initiation phase is accelerated and not presented here).

Another source of error that affects the accuracy of the calculated corrosion current densities, irrespective of the measurement method, is the presence of localized attacks (pitting) which is common in the case of chloride-induced corrosion. In pitting corrosion, the actual area which is being actively corroded is smaller than the total area of the electrode. This means that using the total area of the electrode to calculate the intensity of the corrosion current leads to underestimation of the corrosion current density [42]. This remains a general difficulty in the study of the chloride-induced corrosion using the conventional electrochemical techniques; especially when both localized and general corrosions are available (like in the present study, Section 3-7) and distinguishing between their associated contributions in the total corrosion current density is impossible.

Despite all the inaccuracies associated with measuring the minuscule amount of rust products, measuring the mass difference of the embedded steel before and after submitting the sample to the corrosive conditions is still the most reliable technique to assess the corrosion rate and to validate the results of electrochemical measurements. This mass loss can be directly compared to the mass loss calculated from corrosion current densities using Faraday's law. Fig. 10 compares the gravimetric and electrochemical mass losses of eight GPC samples (each data point is the average of two measurements). Mass loss measurements were conducted after each Tafel test in which the corrosion current density had been measured.

To calculate the electrochemical mass loss using Faraday's law, the area under the average corrosion current density curve vs. time has been integrated and used. During the drying cycles, only a fraction of the area is used (for instance 62.5% for two-weeks-long drying cycles), to take the effect of decreasing corrosion current during the drying cycles into account. To calculate this modification factor for drying cycles, two samples were polarized over a rather limited range of overpotentials ($E\text{-}E_{corr} = -120$ to $+120$ mV) at the end of their wetting cycles and then over the normal range ($E\text{-}E_{corr} = -200$ to $+200$ mV) at the end of their two-weeks drying cycle. The former limited polarization range enables measuring the corrosion current values using the Tafel plot method while minimizing the introduced irreversible changes into the system [44]. Corrosion current densities at the end of the drying cycles were almost 25% of the values recorded at the end of the wetting cycles which means an average decline of about: $[1 - (1 + 0.25) / 2] \times 100 = 37.5\%$ within two weeks of drying.

Results of a comparison between the gravimetric and electrochemical mass losses of bare steel bars embedded in hardened mortar from Andrade & Gonzalez [63] is also presented in Fig. 10 as a benchmark. Andrade & Gonzalez's reported results show a general tendency for the gravimetric mass losses to be larger than the electrochemical mass losses. The authors have claimed that this behavior can be improved by eliminating the effect of uncompensated IR-drop. Nonetheless, the IR-drop is automatically compensated by the potentiostat in the current study (Sections 2-3). Two dashed lines which are parallel to the line of equality are representative of the acceptable scattering range for PCC samples, due to an intrinsic error factor of 2 when the Stern-Geary equation is employed to assess the corrosion current density [42,64]. While all the GPC data points in Fig. 10 scatter in a range which is comparable to the reported acceptable results for Portland cement concrete, they are all lying around the line where the gravimetric mass loss is equal to the electrochemical mass loss. This implies that the employed conventional electrochemical test methods predicted the corrosion rate of the geopolymer-based corroding system with an acceptable level of accuracy. Also, these results confirm the suitability of the selected sweep rates to perform the potentiodynamic tests, as too slow or too fast sweep rates could lead to an underestimation or overestimation of the corrosion current density and hence the calculated electrochemical mass losses.

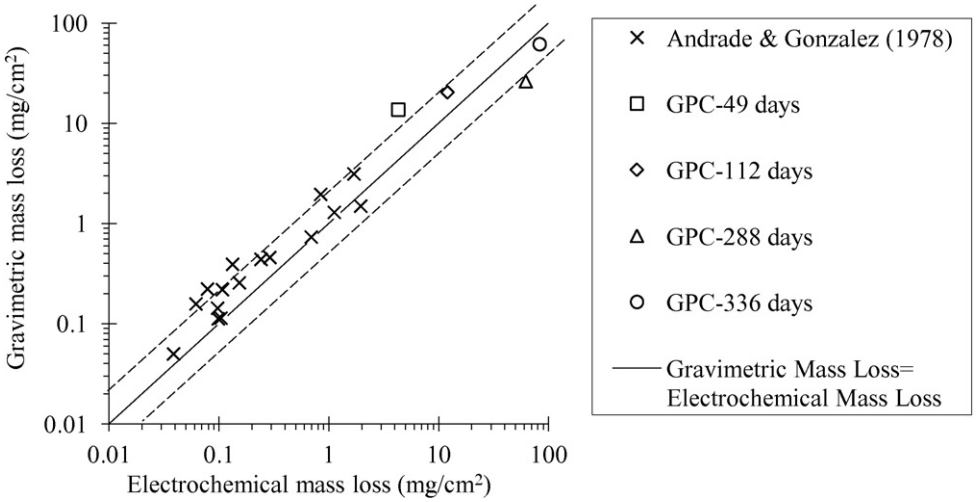

Fig. 10. Gravimetric mass loss vs. electrochemical mass loss for GPC and PCC.

3.7. Corrosion pattern

Fig. 11 shows the corrosion pattern for a sample after experiencing 15 wetting/drying cycles (336 days) in NaCl solution and ambient condition respectively. No corrosion induced crack was observed around the steel bar. The steel bar is gently brushed with a non-metallic bristle to remove loose and bulky corrosion products as well as the loose adherent concrete particles before taking the photo. As it can be seen, a combination of uniform (microcell) and localized (pitting) corrosion is observed, and the pitting attack is concentrated on the lower surface of the reinforcing bar which has the least amount of concrete cover against the chloride penetration. Formation of macrocells between the anodic parts (pits) and the rest of the steel surface (as cathode) increases the corrosion current and decreases the corrosion potential [42]. The employed electrochemical test methods are not capable of quantifying the contribution of the pitting or uniform corrosion in the total measured corrosion parameters. As a result, the measured corrosion parameters such as open circuit corrosion potential and corrosion current densities are representative of the whole electrode surface. The corrosion pattern reported in Fig. 11 is similar to the corrosion pattern observed in Portland cement based concrete beams corroded in natural condition combining uniform and localized (pitting) corrosion [75,76].

4. Conclusion

To investigate different aspects of corrosion of reinforcing bars in low-calcium fly ash-based geopolymer concretes during the propagation phase of corrosion, a set of electrochemical tests are conducted, and parameters such as corrosion potential, polarization resistance, Tafel constants and corrosion current density are investigated. Gravimetric mass loss measurements are utilized as a tool to validate the electrochemical results. The test results led to the following conclusions:

a) By conducting a set of cyclic voltammetry tests, sweep rates of 5 and 10 mV/min for passive and active samples are established and used throughout the experimental investigations (i.e. in potentiodynamic tests). These sweep rates are slow enough to ensure a steady-state condition which is required to avoid overestimation of the corrosion current density. They are also fast enough to avoid altering the electrode equilibrium due to the change in the concentration of ions around the electrode which consequently leads to underestimation of the corrosion current density.
b) Corrosion potential and polarization resistance values after depassivation of the reinforcements fall in the same zone of corrosion risk as expected for Portland cement-based corroding systems. On the other hand, based on the reference classifications commonly

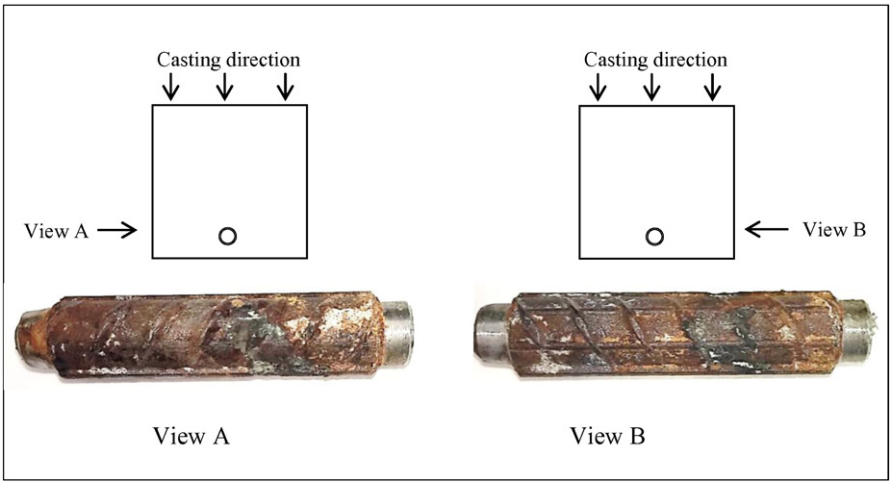

Fig. 11. Corrosion pattern for a sample after 15 wetting/drying cycles (336 days).

used to evaluate the severity of corrosion in reinforced Portland cement concretes, open circuit corrosion potential of passive samples fell in the uncertain to high corrosion risk zones, as opposed to passive/low corrosion risk zone. The lower pH level of the geopolymer binder is considered as the main reasons for the observed low corrosion potential values, although further investigation of the phenomenon is required. Similar behavior was observed for the polarization resistance of the passive samples, where the polarization resistance values were in the low to moderate corrosion risk zones. This finding suggests that the traditional classifications which have been developed for Portland cement-based corroding systems might need some recalibrations to be used for geopolymer-based corroding systems while assessing the passivity of samples.

c) The measured proportionality constants (B), showed a substantial divergence from the conventional values established for Portland cement-based corroding systems (for passive samples: $13 < B < 20$ vs. 52 for PCC, for active specimens after 112 days of wetting-drying in NaCL solution: $45 < B < 58$ vs. 26 for PCC). Using the traditional value of $B = 26$ may lead to underestimation of the corrosion current density of geopolymer-based corroding systems. Although, the approximate inherent of "B″ constant which has resulted in evident discrepancies in the reported values for Portland cement-based corroding systems on the literature, suggests that not all the difference should be attributed to the application of a different binder type. While the values of $B = 52$ and 26 for passive and active Portland-cement based corroding systems are widely accepted as approximate values which provide an accurate enough estimation of the corrosion current density, more experimental results are required for geopolymer-based corroding systems to build up a database of B constants to be used in the Stern-Geary equation.

d) Under the experimental conditions of this study, reinforced low-calcium fly ash-based geopolymer concrete samples exhibit polarization resistance values comparable to Portland cement-based corroding systems. This behavior can be interpreted as a similar electrochemical performance of both binders when used in chloride-contaminated environments.

Acknowledgment

This research work has been supported by the Australian Cooperative Research Centre for Low Carbon Living (grant number RP1020). The experimental work was carried out in the structures laboratory of the School of Civil and Environmental Engineering at the University of New South Wales. The assistance of the laboratory staff is acknowledged here.

References

[1] D.M. Bastidas, A. Fernández-Jiménez, A. Palomo, J.A. González, A study on the passive state stability of steel embedded in activated fly ash mortars, Corros. Sci. 50 (2008) 1058–1065.
[2] M. Taylor, C. Tam, D. Gielen, Energy Efficiency and CO_2 Emissions from the Global Cement Industry, Int Energy Agency, 2006.
[3] P.K. Mehta, Reducing the environmental impact of concrete, Concr. Int. 61–66 (2001).
[4] Broomfield, Corrosion of Steel in Concrete: Understanding, Investigation and Repair, Second Edition [Hardcover], 2 ed. CRC Press, 2006.
[5] M.B. Ali, R. Saidur, M.S. Hossain, A review on emission analysis in cement industries, Renew. Sust. Energ. Rev. 15 (2011) 2252–2261.
[6] ASCE, ASCE, Report card for America's infrastructure, Am. Soc Civ. Eng. (2013).
[7] G.H. Koch, P.H. Brogers, N. Thompson, Y.P. Virmani, J.H. Payer, Corrosion Cost and Preventive Strategies in the United States, Corrosion Cost and Preventive Strategies in the United States, FHWA Report; FHWA-RD-01–156, Washington, DC., 2002
[8] E.J. Wallbank, G.B.D. of Transport, G.M.& Partners, The Performance of Concrete in Bridges: A Survey of 200 Highway Bridges, H.M.S.O., 1989
[9] S.A. Bernal, R. Mejía de Gutiérrez, A.L. Pedraza, J.L. Provis, E.D. Rodriguez, S. Delvasto, Effect of binder content on the performance of alkali-activated slag concretes, Cem. Concr. Res. 41 (2011) 1–8.
[10] J. Davidovits, Geopolymers and geopolymeric materials, J. Therm. Anal. 35 (1989) 429–441, http://dx.doi.org/10.1007/BF01904446.
[11] J. Davidovits, Geopolymer Chemistry and Applications, Geopolymer Institute, 2008.
[12] P. Duxson, J.L. Provis, G.C. Lukey, J.S.J. van Deventer, The role of inorganic polymer technology in the development of "green concrete", Cem. Concr. Res. 37 (2007) 1590–1597.
[13] M. Sofi, J.S.J. van Deventer, P.A. Mendis, G.C. Lukey, Engineering properties of inorganic polymer concretes (IPCs), Cem. Concr. Res. 37 (2007) 251–257.
[14] A.M. Fernández-Jiménez, A. Palomo, C. López-Hombrados, Engineering properties of alkali-activated fly ash concrete, ACI Mater. J. 103 (2006) 106–112.
[15] K. Kupwade-Patil, F. Soto, A. Kunjumon, E.N. Allouche, D.S. Mainardi, Multi-scale modeling and experimental investigations of geopolymeric gels at elevated temperatures, Comput. Struct. 122 (2013) 164–177.
[16] A. Fernandez-Jimenez, I. García-Lodeiro, A. Palomo, Durability of alkali-activated fly ash cementitious materials, J. Mater. Sci. 42 (2006) 3055–3065.
[17] T. Bakharev, Resistance of geopolymer materials to acid attack, Cem. Concr. Res. 35 (2005) 658–670.
[18] T. Bakharev, Durability of geopolymer materials in sodium and magnesium sulfate solutions, Cem. Concr. Res. 35 (2005) 1233–1246.
[19] Y. Fu, L. Cai, W. Yonggen, Freeze–thaw cycle test and damage mechanics models of alkali-activated slag concrete, Constr. Build. Mater. 25 (2011) 3144–3148.
[20] Z. Yunsheng, S. Wei, Fly ash based geopolymer concrete, Indian Concr. J. 80 (2006) 20–24.
[21] J.L. Provis, Y. Muntingh, R.R. Lloyd, H. Xu, L.M. Keyte, L. Lorenzen, et al., Will geopolymers stand the test of time? Dev. Porous, Biol. Geopolymer Ceram. Ceram. Eng. Sci. Proceedings, Vol. 28, Issue 9, John Wiley & Sons, Inc., 2007 235–248.
[22] K. Kupwade-Patil, E.N. Allouche, Examination of chloride-induced corrosion in reinforced geopolymer concretes, J. Mater. Civ. Eng. 25 (2013) 1465–1476, http://dx.doi.org/10.1061/(ASCE)MT.1943-5533.0000672.
[23] Y. Muntingh, Durability and Diffusive Behaviour Evaluation of Geopolymeric Material, 2006.
[24] R.R. Lloyd, J.L. Provis, J.S.J. van Deventer, Pore solution composition and alkali diffusion in inorganic polymer cement, Cem. Concr. Res. 40 (2010) 1386–1392.
[25] J.M. Miranda, A. Fernández-Jiménez, J.A. González, A. Palomo, Corrosion resistance in activated fly ash mortars, Cem. Concr. Res. 35 (2005) 1210–1217.
[26] M. Sufian Badar, K. Kupwade-Patil, S.A. Bernal, J.L. Provis, E.N. Allouche, Corrosion of steel bars induced by accelerated carbonation in low and high calcium fly ash geopolymer concretes, Constr. Build. Mater. 61 (2014) 79–89.
[27] E. Bastidas-Arteaga, P. Bressolette, A. Chateauneuf, M. Sánchez-Silva, Probabilistic lifetime assessment of RC structures under coupled corrosion–fatigue deterioration processes, Struct. Saf. 31 (2009) 84–96.
[28] A. Fernández-Jiménez, J.M. Miranda, J.A. González, A. Palomo, Estabilidad del estado pasivo del acero en morteros de ceniza volante activada, Mater. Constr. 60 (2010) 51–65, http://dx.doi.org/10.3989/mc.2010.53909.
[29] D.V. Reddy, J.-B. Edouard, K. Sobhan, Durability of fly ash–based geopolymer structural concrete in the marine environment, J. Mater. Civ. Eng. 25 (2013) 781–787.
[30] M. Olivia, H. Nikraz, Properties of fly ash geopolymer concrete designed by Taguchi method, Mater. Des. 36 (2012) 191–198.
[31] T.S. Ng, S.J. Foster, Development of a mix design methodology for high-performance geopolymer mortars, Struct. Concr. 14 (2013) 148–156.
[32] A. Palomo, M.W. Grutzeck, M.T. Blanco, Alkali-activated fly ashes, Cem. Concr. Res. 29 (1999) 1323–1329.
[33] D. Hardjito, B.V. Rangan, Development and Properties of Low Calcium Fly Ash Based Geopolymer Concrete, Curtin, Perth, Australia, 2005.
[34] D. Hardjito, S. Wallah, D. Sumajouw, B. Rangan, On the development of fly ash-based geopolymer concrete, ACI Mater. J. 101 (2004) 467–472.
[35] J. Provis, S. Bernal, Geopolymers and related alkali-activated materials, Annu. Rev. Mater. Res. (2014).
[36] A. Nasser, A. Clément, S. Laurens, A. Castel, Influence of steel–concrete interface condition on galvanic corrosion currents in carbonated concrete, Corros. Sci. 52 (2010) 2878–2890.
[37] R. Zhang, A. Castel, R. François, Influence of steel-concrete interface defects owing to the top-bar effect on the chloride-induced corrosion of reinforcement, Mag. Concr. Res. 63 (2011) 773–781.
[38] J.A. Gonzalez, A. Molina, M.L. Escudero, C. Andrade, Errors in the electrochemical evaluation of very small corrosion rates—I. Polarization resistance method applied to corrosion of steel in concrete, Corros. Sci. 25 (1985) 917–930.
[39] I. Martínez, C. Andrade, Polarization resistance measurements of bars embedded in concrete with different chloride concentrations: EIS and DC comparison, Mater. Corros. 62 (2011) 932–942.
[40] A. Castel, A. Nasser, Influence of pre-existing oxides layer and interface condition with carbonated concrete on active reinforcing steel corrosion, Mater. Corros. (2013) (n/a–n/a).
[41] M. Stern, A.L. Geary, Electrochemical polarization: I. A theoretical analysis of the shape of polarization curves, J. Electrochem. Soc. 104 (1957) 56.
[42] C. Andrade, C. Alonso, Corrosion rate monitoring in the laboratory and on-site, Constr. Build. Mater. 10 (1996) 315–328.
[43] A.J. Bard, L.R. Faulkner, Electrochemical Methods: Fundamentals and Applications, Wiley, 2000.
[44] Z.-T. Chang, B. Cherry, M. Marosszeky, Polarisation behaviour of steel bar samples in concrete in seawater. Part 1: experimental measurement of polarisation curves of steel in concrete, Corros. Sci. 50 (2008) 357–364.
[45] J.A. González, J.M. Miranda, N. Birbilis, S. Feliu, Electrochemical techniques for studying corrosion of reinforcing steel: limitations and advantages, Corrosion 61 (2005) 37–50.
[46] BioLogic, EC-lab software, Techniques and Applications (2013) 85.

[47] ASTM, ASTM G1 - 03(2011) standard practice for preparing, cleaning, and evaluating corrosion test specimens, ASTM Int. (2011).
[48] ASTM C1152/C1152M-04(2012)e1, Standard Test Method for Acid-soluble Chloride in Mortar and Concrete, http://www.astm.org/Standards/C1152.htm (n.d. accessed October 1, 2015).
[49] V. Räsänen, V. Penttala, The pH measurement of concrete and smoothing mortar using a concrete powder suspension, Cem. Concr. Res. 34 (2004) 813–820, http://dx.doi.org/10.1016/j.cemconres.2003.09.017.
[50] R.S. Barneyback, S. Diamond, Expression and analysis of pore fluids from hardened cement pastes and mortars, Cem. Concr. Res. 11 (1981) 279–285, http://dx.doi.org/10.1016/0008-8846(81)90069-7.
[51] ACI, ACI committee 222: corrosion of metal in concrete, Concr. Int. 7 (1985) 56–59.
[52] RILEM, RILEM technical committee 124-SRC: draft recommendation for repair strategies for concrete structures damaged by reinforcement corrosion, Mater. Struct. 27 (1994) 415–436, http://dx.doi.org/10.1007/BF02473446.
[53] J.A. González, A. Molina, M.L. Escudero, C. Andrade, Errors in the electrochemical evaluation of very small corrosion rates—II. Other electrochemical techniques applied to corrosion of steel in concrete, Corros. Sci. 25 (1985) 519–530.
[54] ASTM, ASTM C876 - 09 standard test method for corrosion potentials of uncoated reinforcing steel in concrete, ASTM Int. (2009).
[55] ASTM, ASTM G3-14 (2014) standard practice for conventions applicable to electrochemical measurements in corrosion testing, ASTM Int. (2014).
[56] I.A. Ammar, S. Riad, Effect of pH on corrosion potentials, J. Phys. Chem. 62 (1958) 150–154, http://dx.doi.org/10.1021/j150560a004.
[57] H.R. Soleymani, M.E. Ismail, Comparing corrosion measurement methods to assess the corrosion activity of laboratory OPC and HPC concrete specimens, Cem. Concr. Res. 34 (2004) 2037–2044.
[58] A. Poursaee, C.M. Hansson, Potential pitfalls in assessing chloride-induced corrosion of steel in concrete, Cem. Concr. Res. 39 (2009) 391–400.
[59] B. Elsener, C. Andrade, J. Gulikers, R. Polder, M. Raupach, Hall-cell potential measurements—potential mapping on reinforced concrete structures, Mater. Struct. 36 (2003) 461–471.
[60] P. Ghods, O.B. Isgor, G.A. McRae, G.P. Gu, Electrochemical investigation of chloride-induced depassivation of black steel rebar under simulated service conditions, Corros. Sci. 52 (2010) 1649–1659.
[61] V. Garcia, R. François, M. Carcasses, P. Gegout, Potential measurement to determine the chloride threshold concentration that initiates corrosion of reinforcing steel bar in slag concretes, Mater. Struct. 47 (2013) 1483–1499.
[62] S. Millard, D. Law, J. Bungey, J. Cairns, Environmental influences on linear polarisation corrosion rate measurement in reinforced concrete, NDT E Int. 34 (2001) 409–417.
[63] C. Andrade, J.A. Gonzalez, Quantitative measurements of corrosion rate of reinforcing steels embedded in concrete using polarization resistance measurements, Mater. Corros. Korros. 29 (1978) 515–519.
[64] F. Mansfeld, K.B. Oldham, A modification of the Stern—Geary linear polarization equation, Corros. Sci. 11 (1971) 787–796, http://dx.doi.org/10.1016/S0010-938X(71)80012-4.
[65] G. Song, Theoretical analysis of the measurement of polarisation resistance in reinforced concrete, Cem. Concr. Compos. 22 (2000) 407–415, http://dx.doi.org/10.1016/S0958-9465(00)00040-8.
[66] C.E. Locke, A. Siman, Electrochemistry of reinforcing steel in salt-contaminated concrete, corrosion of reinforcing steel in concrete, ASTM International (1980).
[67] F. MANSFELD, The effect of uncompensated IR-drop on polarization resistance measurements, Corrosion 32 (1976) 143–146, http://dx.doi.org/10.5006/0010-9312-32.4.143.
[68] C. Dehghanian, The Electrochemical Behavior of Steel in Salt-Contaminated Concrete, Univ. Oklahoma, 1980 (Available from ProQuest Diss. Theses Glob. (303070358) http://search.proquest.com/dissertations/docview/303070358/4C0356ECA1A4923PQ/2?accountid=12763 (accessed May 9, 2016).
[69] C. Alonso, C. Andrade, X. Nóvoa, M. Izquierdo, M. Pérez, Effect of protective oxide scales in the macrogalvanic behaviour of concrete reinforcements, Corros. Sci. 40 (1998) 1379–1389, http://dx.doi.org/10.1016/S0010-938X(98)00040-7.
[70] A. Bentur, N. Berke, S. Diamond, Steel Corrosion in Concrete: Fundamentals and Civil Engineering Practice, CRC Press, 1997.
[71] E. Heitz, W. Schwenk, Theoretical Basis for the Determination of Corrosion Rates from Polarisation Resistance: Report Prepared for the European Federation of Corrosion Working Party on "Physicochemical Testing Methods of Corrosion—Fundamentals and Application", 2013.
[72] L.M. Callow, J.A. Richardson, J.L. Dawson, Corrosion monitoring using polarisation resistance measurements: I. Techniques and correlations, Br. Corros. J. 11 (1976) 123–131, http://dx.doi.org/10.1179/000705976798319937.
[73] L.M. Callow, J.A. Richardson, J.L. Dawson, Corrosion monitoring using polarisation resistance measurements: II. Sources of error, Br. Corros. J. 11 (1976) 132–139, http://dx.doi.org/10.1179/000705976798320070.
[74] C. Alonso, C. Andrade, X. Nóvoa, M. Izquierdo, M. Pérez, Effect of protective oxide scales in the macrogalvanic behaviour of concrete reinforcements, Corros. Sci. 40 (1998) 1379–1389, http://dx.doi.org/10.1016/S0010-938X(98)00040-7.
[75] G. Arliguie, A. Castel, T. Vidal, R. François, Influence of steel–concrete interface quality on reinforcement corrosion induced by chlorides, Mag. Concr. Res. 55 (2003) 151–159, http://dx.doi.org/10.1680/macr.2003.55.2.151.
[76] R.J. Zhang, A. Castel, R. François, Effect of steel corrosion pattern on RC beam performance, Proc. ICE - Constr. Mater. 163 (2010) 97–108, http://dx.doi.org/10.1680/coma.2010.163.2.97.